# Robust Trajectory Tracking Control for Underactuated Autonomous Underwater Vehicles

Shahab Heshmati-alamdari, Alexandros Nikou and Dimos V. Dimarogonas

*Abstract*— **This paper addresses the tracking control problem of 3D trajectories for underactuated underwater robotic vehicles operating in an uncertain workspace including obstacles. In particular, a robust Nonlinear Model Predictive Control (NMPC) scheme is presented for the case of underactuated Autonomous Underwater Vehicles (AUVs) (i.e., vehicles actuated only in surge, heave and yaw). The purpose of the controller is to steer the underactuated AUV to a desired trajectory with guaranteed input and state constraints inside a dynamic environment where the knowledge of the operating workspace is constantly updated on–line via the vehicle's on–board sensors. In particular, obstacle avoidance with any of the detected obstacles is guaranteed, despite the model dynamic uncertainties and the presence of external disturbances representing ocean currents and waves. The proposed feedback control law consists of two parts: an online law which is the outcome of a Finite Horizon Optimal Control Problem (FHOCP) solved for the nominal dynamics; and a state feedback law which is tuned off-line and guarantees that the real trajectories remain bounded in a hyper-tube centered along the nominal trajectories for all times. Finally, a simulation study verifies the performance and efficiency of the proposed approach.**

## I. Introduction

During the last decades, considerable progress has been made in the field of unmanned marine vehicles, with a significant number of results in a variety of marine activities (e.g., ocean forecasting, underwater inspection of oil/gas pipelines) [1]. A typical marine control problem is trajectory tracking which aims to steer the Autonomous Underwater Vehicle on a reference trajectory. Classical approaches such as local linearization and input-output decoupling have been used in the past to design motion controllers for underwater vehicles. Nevertheless, the aforementioned methods yielded poor closed-loop performance and the results were local, around only certain selected operating points. Output feedback linearization [2] is an alternative approach which however is not always possible. Moreover, based on a combined approach involving Lyapunov theory and backstepping, various model-based non-linear controllers have been proposed in the literature [3].

Dynamic model uncertainties of underwater robotic vehicles have been mainly compensated by employing adaptive control techniques. In addition, for all of the aforementioned motion control strategies, it is not always feasible or straightforward to incorporate control input and state constraints into the vehicle's closed-loop motion. In that sense, the motion control problem of underwater robots continues to pose considerable challenges to system designers, especially in view of the high-demanding underwater missions.

On the other hand, the reference trajectory for the underwater robot is usually the result of some path planning techniques [4]. The majority of planning techniques are based on off–line optimization schemes, which consider static or quasi–static operational environments. However, in real–time missions, the vehicle operates in a partially known and dynamic environment where the knowledge of the operating workspace is constantly updated on–line via the vehicle's on–board sensors (e.g., multi-beam imaging sonars, on-line ocean current estimators). In these cases, the underwater vehicle has to re-calculate its path on–line according to possible environmental changes (i.e., new obstacles).

Motivated by the aforementioned considerations, this work presents a robust trajectory tracking control scheme for underactuated Autonomous Underwater Vehicles (AUVs) operating in a constrained workspace including obstacles. In particular, a robust Nonlinear Model Predictive Control (NMPC) scheme is presented for the underactuated AUVs (i.e., vehicles actuated only in surge, heave and yaw). Various constraints such as: sparse obstacles, workspace boundaries, control input saturation are considered during the control design. The purpose of the controller is to steer the underactuated AUV on a desired trajectory inside a constrained and dynamic workspace. Since the knowledge of the operating workspace is constantly updated online via the vehicle's on–board sensors, the robot re-calculates its path online if the updated environmental changes (i.e., new detected obstacles) are in conflict with the reference trajectory. In particular, by considering a ball which covers the volume of the system, obstacle avoidance with any of the detected obstacles is guaranteed, despite the model dynamic uncertainties and the presence of external disturbances representing ocean currents and waves. The proposed feedback control law consists of two parts: an online law which is the outcome of a Finite Horizon Optimal Control Problem (FHOCP) solved for the nominal dynamics; and a state feedback law which is tuned off-line and guarantees that the real trajectories remain bounded in a hyper-tube centered along the nominal trajectories for all times. The closed-loop system has analytically guaranteed stability and convergence properties. A more detailed version of this paper that contains material that has been omitted due to space constraints can be found in [5].

Division of Decision and Control Systems, School of Electrical Engineering and Computer Science, KTH Royal Institute of Technology, Stockholm, Sweden, E-mail: {shaha, anikou, dimos}@kth.se.
This work was supported by the H2020 ERC Grant BUCOPHSYS, the Swedish Foundation for Strategic Research (SSF), the Swedish Research Council (VR) and the Knut och Alice Wallenberg Foundation (KAW).

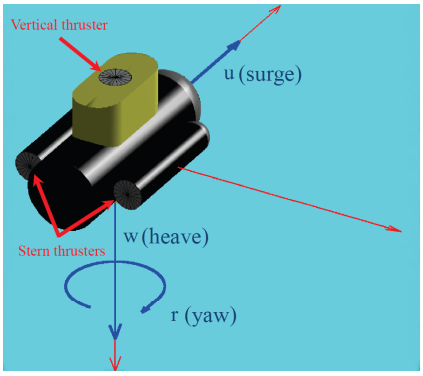


**Fig. 1:** The underactuated underwater vehicle. Blue color indicates the actuated degrees of freedom.

## II. Notations

Define by $\mathbb{N}$ and $\mathbb{R}$ the sets of positive integers and real numbers, respectively. Given a set $\mathcal{S}$, denote by $|\mathcal{S}|$ and $\mathcal{S}^n := \mathcal{S} \times \cdots \times \mathcal{S}$ its cardinality and its $n$-fold Cartesian product. Given a vector $\boldsymbol{z} \in \mathbb{R}^n$ define by:

$$\|\boldsymbol{z}\|_2 := \sqrt{\boldsymbol{z}^\top \boldsymbol{z}}, \quad \|\boldsymbol{z}\|_\infty := \max_{i=1,\dots,n} |\boldsymbol{z}_i|, \quad \|\boldsymbol{z}\|_P := \sqrt{\boldsymbol{z}^\top \boldsymbol{P} \boldsymbol{z}},$$

its Euclidean, infinite and $\boldsymbol{P}$-weighted norm, respectively, with $\boldsymbol{P} \geq 0$. The notation $\lambda_{\min}(\boldsymbol{P})$ stands for the minimum absolute value of the real part of the eigenvalues of $\boldsymbol{P} \in \mathbb{R}^{n\times n}$; $0_{m\times n} \in \mathbb{R}^{m\times n}$ and $I_n \in \mathbb{R}^{n\times n}$ stand for the $m \times n$ matrix with all entries zeros and the identity matrix, respectively. The notation $\text{diag}\{P_1, \dots, P_n\}$ stands for the block diagonal matrix with the matrices $P_1, \dots, P_n$ in the main diagonal;

$$\mathcal{B}(\boldsymbol{c}, r) := \{\boldsymbol{x} \in \mathbb{R}^n : \|\boldsymbol{x} - \boldsymbol{c}\|_2 \leq r\},$$

stands for a ball in $\mathbb{R}^n$ with center and radius $\boldsymbol{c} \in \mathbb{R}^n$, $r > 0$, respectively. Given sets $\mathcal{S}_1$, $\mathcal{Z} \subseteq \mathbb{R}^n$, $\mathcal{S}_2 \subseteq \mathbb{R}^m$ and matrix $\boldsymbol{P} \in \mathbb{R}^{n\times m}$, the *Minkowski addition*, the *Pontryagin difference* and the *matrix-set multiplication* are respectively defined by:

$$\begin{aligned}
\mathcal{S}_1 \oplus \mathcal{Z} &:= \{\boldsymbol{s}_1 + \boldsymbol{z} : \boldsymbol{s}_1 \in \mathcal{S}_1, \boldsymbol{z} \in \mathcal{Z}\},\\
\mathcal{S}_1 \ominus \mathcal{Z} &:= \{\boldsymbol{s}_1 \in \mathcal{S}_1 : \boldsymbol{s}_1 + \boldsymbol{z} \in \mathcal{S}_1, \forall \boldsymbol{z} \in \mathcal{Z}\},\\
P \circ \mathcal{S}_2 &:= \{\boldsymbol{P}\boldsymbol{s}, \boldsymbol{s} \in \mathcal{S}_2\}.
\end{aligned}$$

## III. Problem Statement

### A. Mathematical Modeling

The pose vector of the vehicle with respect to (w.r.t.) the inertial frame $\mathcal{I}$ is denoted by $\boldsymbol{\eta} = \begin{bmatrix}\boldsymbol{\eta_1^T} & \boldsymbol{\eta_2^T}\end{bmatrix}^T \in \mathbb{R}^6$ including the position (i.e., $\boldsymbol{\eta_1} = [x\ y\ z]^T$) and orientation (i.e., $\boldsymbol{\eta_2} = [\phi\ \theta\ \psi]^T$) vectors. The $\boldsymbol{v} = \begin{bmatrix}\boldsymbol{v_1^T} & \boldsymbol{v_2^T}\end{bmatrix}^T \in \mathbb{R}^6$ is the velocity vector of the vehicle expressed in body fixed frame $\mathcal{V}$ and includes the linear (i.e., $\boldsymbol{v_1} = [u\ v\ w]^T$) and angular (i.e., $\boldsymbol{v_2} = [p\ q\ r]^T$) velocity vectors where the components have been named according to SNAME [6] as surge, sway, heave, roll, pitch and yaw respectively (Fig.1).

We assume that the considered underwater vehicle is equipped with three thrusters, which are effective only in surge, heave and yaw motion (Fig.1), meaning that the vehicle is under-actuated along the sway axis. Moreover, we assume that the vehicle is designed with meta-centric restoring forces in order to regulate roll and pitch angles. Thus, the angles $\phi$, $\theta$ and angular velocities $p$ and $q$ are negligible and we can consider them to be equal to zero. Thus, from now on, we denote by $\boldsymbol{x} = [x, y, z, \psi]^\top$ and $\boldsymbol{v} = [u, w, r]^\top$ the state and the control input of the system respectively. The vehicle is symmetric around the $x$ - $z$ plane and close to symmetric around the $y$ - $z$ plane. Therefore, we can safely assume that motions in heave, roll and pitch are decoupled [7]. Because the vehicle is operating at relatively low speeds, the coupling effects are considered to be negligible. Due to the above assumptions and the relative low speed of the vehicle, we consider the vehicle's motion equations, which given as follows:

$$\dot{\boldsymbol{x}} = f(\boldsymbol{x})\boldsymbol{v} + g(\boldsymbol{x}, v) \tag{1}$$

where $\dot{\boldsymbol{x}} = [\dot{x},\ \dot{y},\ \dot{z},\ \dot{\psi}]^\top$ and:

$$f(\boldsymbol{x})\boldsymbol{v} = \begin{bmatrix}\cos(\psi) & 0 & 0\\ \sin(\psi) & 0 & 0\\ 0 & 1 & 0\\ 0 & 0 & 1\end{bmatrix}\begin{bmatrix}u\\ w\\ r\end{bmatrix}, \quad g(\boldsymbol{x}, v) = \begin{bmatrix}-\sin(\psi)\\ \cos(\psi)\\ 0\\ 0\end{bmatrix} v$$

Notice that the $v$ indicates the vehicle velocity in the sway direction. In [8], using Input-to-State Stability (ISS) framework, it was shown that for any vehicle described by (1) and for any bounded control input $[u, r]$ the velocity around the sway direction $v$ can be seen as a bounded perturbation with upper bound $||v|| \leq \bar{v}$. Note that throughout this paper the notation $(\ \bar{\cdot}\ )$ will denote the upper bound for each of the variables. Therefore we consider the system:

$$\dot{\boldsymbol{x}} = f(\boldsymbol{x})\boldsymbol{v} \tag{2}$$

as the nominal kinematic system of the underwater vehicle, while the function $g(\cdot)$ is considered as a bounded inner disturbance of the system that vanishes at the origin. Also, $g(\boldsymbol{x}, v) \in \Gamma \subset \mathbb{R}^4$ with $\Gamma$ being a compact set, such that:

$$||g(\boldsymbol{x}, v)|| \leq \bar{\gamma} \quad \text{with} \quad \bar{\gamma} \triangleq \bar{v} \tag{3}$$

The robot moves under the influence of an irrotational current which behaves as an external disturbance. The current has components with respect to the $x$, $y$ and $z$ axes, denoted by $\delta_x$, $\delta_y$ and $\delta_z$, respectively. Also it is assumed to have a slowly-varying velocity $\delta_c$ which is upper bounded by $||\delta_c|| \leq \bar{\delta}_c$ and it has direction $\beta$ in the $x-y$ plane and $\alpha$ with respect to the $z$-axis of the global frame. In particular we set $\delta = [\delta_x, \delta_y, \delta_z, 0]^\top \in \Delta \subset \mathbb{R}^4$ with $\Delta$ being a compact set, where:

$$\begin{aligned}
\delta_x &\triangleq \delta_c \cos(\beta)\sin(\alpha)\\
\delta_y &\triangleq \delta_c \sin(\beta)\sin(\alpha)\\
\delta_z &\triangleq \delta_c \cos(\alpha)
\end{aligned} \tag{4}$$

It is easy to show that there exists a $\bar{\delta} > 0$ such that $||\delta|| \leq \bar{\delta}$. Taking into consideration the aforementioned disturbances

that affect the vehicle, we can model the perturbed system as follows:

$$\dot{\boldsymbol{x}} = f(\boldsymbol{x})\boldsymbol{v} + \boldsymbol{\omega} \tag{5}$$

with $\boldsymbol{\omega} = [\omega_1,\ \omega_2,\ \omega_3,\ 0]^\top \coloneqq g(\boldsymbol{x}, v) + \delta \in \Omega \subset \mathbb{R}^4$ as the result of adding the inner and external disturbances of the system and $\Omega$ is a compact set with $\Omega = \Delta \oplus \Gamma$. Since the sets $\Delta$ and $\Gamma$ are compact, we have that $\Omega$ is also a compact set, and thus we have:

$$\Omega = \{\boldsymbol{\omega}(t) \in \mathbb{R}^4 : ||\boldsymbol{\omega}(t)||_2 \leq \bar{\omega}\} \tag{6}$$

with $\bar{\omega} \triangleq \bar{\delta} + \bar{\gamma}$ .

### B. Geometry of the Workspace

We consider that the underwater vehicle operates inside a workspace $\mathcal{W} \subset \mathbb{R}^3$ with boundary $\partial\mathcal{W}$ and scattered obstacles located within it. Without loss of the generality, the robot and the obstacles are modeled by spheres (i.e., we adopt the spherical world representation [9]). Let $\mathcal{B}(\boldsymbol{\eta}_1, \bar{r})$ be a closed ball that covers the whole vehicle volume (main body and additional equipments). Moreover, let $\mathcal{B}(\boldsymbol{\eta}_1, \bar{R})$ with $\bar{R} > \bar{r}$ be a sensing area where the robot can perceive and update its knowledge of the workspace (i.e., the obstacle locations) using its on-board sensors. Furthermore, the $\mathcal{M}$ static obstacles within the workspace are defined as closed balls described by $\pi_m = \mathcal{B}(\boldsymbol{p}_{\pi_m}, r_{\pi_m}),\ m \in \{1, \ldots, \mathcal{M}\}$, where $\boldsymbol{p}_{\pi_m} \in \mathbb{R}^3$ is the center and $r_{\pi_m} > 0$ the radius of the obstacle $\pi_m$. Additionally, based on the property of spherical world [9], it holds that there exists a feasible trajectory $\boldsymbol{\eta}(t)$ for the vehicle such as:

$$\mathcal{B}(\boldsymbol{\eta}_1(t), \bar{r}) \cap \{\mathcal{B}(\boldsymbol{p}_{\pi_m}, r_{\pi_m}) \cup \partial\mathcal{W}\} = \emptyset, \quad \forall t \geq 0, \forall m \in \{1, \ldots, \mathcal{M}\} \tag{7}$$

### C. Constraints

*1) State Constraints:* The obstacle avoidance requirement is captured by the state constraint set $X$ of the system, given by:

$$\boldsymbol{x}(t) \in X \subset \mathbb{R}^4 \tag{8}$$

which in view of (7) can be defined as:

$$X \coloneqq \Big\{\boldsymbol{x} \in \mathbb{R}^4 : \mathcal{B}(\boldsymbol{\eta}_1, \bar{r}) \cap \{\mathcal{B}(\boldsymbol{p}_{\pi_m}, r_{\pi_m}) \cup \partial\mathcal{W}\} = \emptyset, \quad \forall m \in \{1, \ldots, \mathcal{M}\}\Big\} \tag{9}$$

*2) Input Constraints:* for the needs of several common underwater tasks (e.g., seabed inspection, mosaicking), the vehicle is required to move with relatively low speeds with upper bound denoted by the velocity vector $\bar{\boldsymbol{v}} = [\bar{u}\ \bar{w}\ \bar{r}]^\top$ which defines the control constraint set $V$ as follows:

$$\boldsymbol{v}(t) \in V \subseteq \mathbb{R}^3 \tag{10}$$

These constraints are of the form $|u(t)| \leq \bar{u}$ , $|w(t)| \leq \bar{w}$, $|r(t)| \leq \bar{r}$, that is:

$$V \coloneqq \Big\{\boldsymbol{v} \in \mathbb{R}^3 : \|\boldsymbol{v}\|_\infty \leq \bar{V}\Big\} \tag{11}$$

with $\bar{V} = (\bar{u}^2 + \bar{w}^2 + \bar{r}^2)^{\frac{1}{2}}$.

### D. Control Objective

The problem of this paper can be defined as follows:

***Problem 1:*** (Robust Tracking Control for an Autonomous Underactuated Underwater Vehicle): Consider an Underactuated Autonomous Underwater Vehicle described by (5) operating in a workspace $\mathcal{W} \subset \mathbb{R}^3$ with state, input constraints as well as disturbances imposed by the sets $X$, $V$ and $\Omega$ as in (8), (10) and (6), respectively. Consider also that the robot and the obstacles are all modeled according to the spherical world representation and the knowledge of the operating workspace $\mathcal{W}$ is constantly updated via the vehicle's on–board sensors inside a sensing region defined by $\mathcal{B}(\boldsymbol{\eta}_1, \bar{R})$. Given a desired trajectory $\boldsymbol{p}_d(t) = [x_d(t), y_d(t), z_d(t)]^T$, design a feedback control law $\boldsymbol{v} = \kappa(\boldsymbol{x})$ such that the desired trajectory $\boldsymbol{p}_d(t)$ is tracked with guaranteed input and state constraints while avoiding any collision with the detected obstacles, despite the presence of exogenous disturbances representing ocean currents and waves.

## IV. Main Results

In this section we present the methodology proposed in order to formulate the solution of Problem-1. In particular, a Nonlinear Model Predictive Control (NMPC) framework [10], [11] is utilized, and a relevant robust NMPC analysis, the so-called tube-based approach is provided. First we begin by defining the error states and the corresponding transformed constraints.

### A. Error Definitions

Given the desired trajectory $\boldsymbol{p}_d(t) = [x_d(t), y_d(t), z_d(t)]^T$, let us define the position errors:

$$e_x(t) = x - x_d(t),\ e_y(t) = y - y_d(t),\ e_z(t) = z - z_d(t) \tag{12}$$

the projected on the horizontal plane distance error:

$$e_d(t) = \sqrt{e_x^2(t) + e_y^2(t)} \tag{13}$$

as well as the projected on the horizontal plane orientation error:

$$e_o(t) = \frac{e_y(t)}{e_d(t)} c_{\psi(t)} - \frac{e_x(t)}{e_d(t)} s_{\psi(t)} \tag{14}$$

where $s_\star = \sin(\star)$ and $c_\star = \cos(\star)$. It should be noted that the tracking control problem is solved if the projected on the horizontal plane distance error $e_d$, the vertical error $e_z$ and the orientation error $e_o$ reduce to zero. Moreover, the orientation error $e_o$ is well-defined only for nonzero values of $e_d$. For this respect, the proposed approach has been designed to further guarantee that $e_d(t) \geq \epsilon, \forall t \geq 0$, where $\epsilon$ is an arbitrarily small positive value, that avoids the aforementioned singularity issue when $e_d \to 0$. Therefore, in view of (13) and considering the state constraint set $X$ of (8), we can define a feasible error set given as:

$$\mathcal{E} \coloneqq \{\boldsymbol{x} \in X : \sqrt{e_x^2(t) + e_y^2(t)} \geq \epsilon,\ \text{with } \epsilon > 0\} \tag{15}$$

Now, differentiating the aforementioned errors of (12)-(14) and employing (5), we arrive at:

$$\dot{e}_d = \frac{e_x c_\psi + e_y s_\psi}{e_d} u - \frac{e_x \dot{x}_d + e_y \dot{y}_d}{e_d} + \frac{e_x \omega_1 + e_y \omega_2}{e_d} \quad (16)$$

$$\dot{e}_z = w - \dot{z}_d + \omega_3 \quad (17)$$

$$\dot{e}_o = -\frac{[e_y c_\psi - e_x s_\psi][e_x c_\psi + e_y s_\psi]}{e_d^2} u + \frac{e_y \omega_1 - e_x \omega_2}{e_d^2} s_\psi c_\psi - \Big[\frac{e_x}{e_d} c_\psi + \frac{e_y}{e_d} s_\psi\Big] r + \frac{\dot{x}_d}{e_d}\Big[e_o \frac{e_x}{e_d} + s_\psi\Big] + \frac{\dot{y}_d}{e_d}\Big[e_o \frac{e_y}{e_d} - c_\psi\Big] \quad (18)$$

By defining the error vector $\boldsymbol{e} = [e_d,\ e_z,\ e_o]^\top$, the aforementioned formulas can be written in matrix form as:

$$\dot{\boldsymbol{e}} = J(\boldsymbol{e}, \boldsymbol{p}_d)\boldsymbol{v} + \zeta(\boldsymbol{e}, \dot{\boldsymbol{p}}_d) + \xi(\boldsymbol{e}, \boldsymbol{\omega}) \quad (19)$$

where:

$$J(\boldsymbol{e}, \boldsymbol{p}_d)\boldsymbol{v} := \begin{bmatrix} \frac{e_x c_\psi + e_y s_\psi}{e_d} & 0 & 0 \\ 0 & 1 & 0 \\ \frac{[e_y c_\psi - e_x s_\psi][e_x c_\psi + e_y s_\psi]}{e_d^2} & 0 & -\big[\frac{e_x}{e_d} c_\psi + \frac{e_y}{e_d} s_\psi\big] \end{bmatrix} \begin{bmatrix} u \\ w \\ r \end{bmatrix}$$

$$\zeta(\boldsymbol{e}, \dot{\boldsymbol{p}}_d) := \begin{bmatrix} -\frac{e_x \dot{x}_d + e_y \dot{y}_d}{e_d} \\ -\dot{z}_d \\ \frac{e_o(\dot{x}_d e_x + \dot{y}_d e_y) + e_d(s_\psi - c_\psi)}{e_d^2} \end{bmatrix}, \ \xi(\boldsymbol{e}, \boldsymbol{\omega}) := \begin{bmatrix} \frac{e_x \omega_1 + e_y \omega_2}{e_d} \\ \omega_3 \\ \frac{(e_y \omega_1 - e_x \omega_2) s_\psi c_\psi}{e_d^2} \end{bmatrix}$$

which are the uncertain error dynamics of the underwater vehicle system. The corresponding nominal error dynamics can be now given by:

$$\dot{\hat{\boldsymbol{e}}} = J(\hat{\boldsymbol{e}}, \boldsymbol{p}_d)\hat{\boldsymbol{v}} + \zeta(\hat{\boldsymbol{e}}, \dot{\boldsymbol{p}}_d) \quad (20)$$

It should be noticed that we use the $\hat{\boldsymbol{e}}$ notation for the nominal error state in order to account for the mismatch between the real error state and the nominal one which will be used in the following analysis.

**Remark 1:** It should be noted that the constraint set $\mathcal{E}$ in (15) guarantees that $J(\cdot)$ is non-singular. Thus, there exists a strictly positive constant $\underline{J}$ such that: $\lambda_{\min}\left(\frac{J(\cdot)+J^\top(\cdot)}{2}\right) \geq \underline{J} > 0$.

**Remark 2:** It can easily be shown that the function $\xi(\boldsymbol{e}, \boldsymbol{\omega})$ appearing in (19) is a bounded function and there exists a strictly positive constant $\tilde{\xi}$ such that: $||\xi(\boldsymbol{e}, \boldsymbol{\omega})|| \leq \tilde{\xi}$, $\tilde{\xi} > 0$. In particular, by noting that $\frac{|e_x|}{\sqrt{e_x^2+e_y^2}} \leq 1$, $\frac{|e_y|}{\sqrt{e_x^2+e_y^2}} \leq 1$ and $|s_\psi| \leq 1$, $|c_\psi| \leq 1$, we deduce that $\tilde{\xi}$ does not depend of the bounds of $\boldsymbol{e}$.

### *B. State Feedback Design*

Consider the feedback law:

$$\boldsymbol{v} = \hat{\boldsymbol{v}}(\hat{\boldsymbol{e}}) + \kappa(\boldsymbol{e}, \hat{\boldsymbol{e}}) \quad (21)$$

which consists of a nominal control action $\hat{\boldsymbol{v}}(\hat{\boldsymbol{e}}) \in V$ and a state feedback law $\kappa : \mathbb{R}^3 \times \mathbb{R}^3 \to V$. The control action $\hat{\boldsymbol{v}}(\hat{\boldsymbol{e}})$ will be the outcome of a FHOCP solved for the nominal dynamics (20) while the state feedback law $\kappa(\cdot)$ is designed in order to guarantee that the real trajectory $\boldsymbol{e}(t)$ (i.e., the solution of (19)) always remain inside a bounded tube centered along the nominal trajectory $\hat{\boldsymbol{e}}(t)$ i.e., the solution

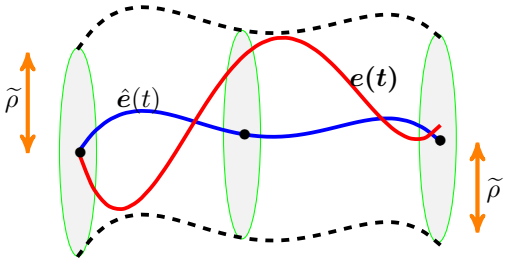


**Fig. 2:** The hyper-tube centered along the trajectory $\hat{\boldsymbol{e}}(t)$ (depicted by the blue line) with radius $\widetilde{\rho}$. The real trajectory $\boldsymbol{e}(t)$ lies inside the hyper-tube for all times.

of (20). Now let us define by $\boldsymbol{z}(t) = [z_1(t),\ z_2(t),\ z_3(t)]^\top$, and then the deviation between the real error state and the nominal one is given as:

$$\boldsymbol{\rho}(t) := \boldsymbol{e}(t) - \hat{\boldsymbol{e}}(t) \quad (22)$$

with $\boldsymbol{\rho}(0) = \boldsymbol{e}(0) - \hat{\boldsymbol{e}}(0) = \boldsymbol{0}$. In view of (22), the dynamics of $\boldsymbol{\rho}(t)$ can be given as:

$$\begin{aligned} \dot{\boldsymbol{\rho}} &= \dot{\boldsymbol{e}} - \dot{\hat{\boldsymbol{e}}} \\ &= J(\boldsymbol{e}, \boldsymbol{p}_d)\boldsymbol{v} - J(\hat{\boldsymbol{e}}, \boldsymbol{p}_d)\hat{\boldsymbol{v}} + \zeta(\boldsymbol{e}, \dot{\boldsymbol{p}}_d) - \zeta(\hat{\boldsymbol{e}}, \dot{\boldsymbol{p}}_d) + \xi(\boldsymbol{e}, \boldsymbol{\omega}). \end{aligned}$$

By adding and subtracting the term $J(\boldsymbol{e}, \boldsymbol{p}_d)\hat{\boldsymbol{v}}$ and by defining the function $h(\boldsymbol{e}, \hat{\boldsymbol{v}}) := J(\boldsymbol{e}, \boldsymbol{p}_d)\hat{\boldsymbol{v}}$, the latter becomes:

$$\begin{aligned} \dot{\boldsymbol{\rho}} = {} & h(\boldsymbol{e}, \hat{\boldsymbol{v}}) - h(\hat{\boldsymbol{e}}, \hat{\boldsymbol{v}}) + J(\boldsymbol{e}, \boldsymbol{p}_d)(\boldsymbol{v} - \hat{\boldsymbol{v}}) \\ & + \zeta(\boldsymbol{e}, \dot{\boldsymbol{p}}_d) - \zeta(\hat{\boldsymbol{e}}, \dot{\boldsymbol{p}}_d) + \xi(\boldsymbol{e}, \boldsymbol{\omega}). \end{aligned} \quad (23)$$

Note that for the continuously differentiable functions $h(\cdot)$ and $\zeta(\cdot)$ the following hold:

$$\|h(\boldsymbol{e}, \hat{\boldsymbol{v}}) - h(\hat{\boldsymbol{e}}, \hat{\boldsymbol{v}})\| \leq \mathcal{L}_1 \|\boldsymbol{e} - \hat{\boldsymbol{e}}\| = \mathcal{L}_1 \|\boldsymbol{\rho}\|, \quad (24a)$$

$$\|\zeta(\boldsymbol{e}, \dot{\boldsymbol{p}}_d) - \zeta(\hat{\boldsymbol{e}}, \dot{\boldsymbol{p}}_d)\| \leq \mathcal{L}_2 \|\boldsymbol{e} - \hat{\boldsymbol{e}}\| = \mathcal{L}_2 \|\boldsymbol{\rho}\|, \quad (24b)$$

where $\mathcal{L}_1,\ \mathcal{L}_2 > 0$ stand for their Lipschitz constants. Now based on the aforementioned analysis the following Lemma can be stated:

**Lemma 1:** The state feedback law designed by:

$$\kappa(\boldsymbol{e}, \hat{\boldsymbol{e}}) := -\sigma(\boldsymbol{e} - \hat{\boldsymbol{e}}), \quad (25)$$

where $\sigma$ is chosen such that:

$$\sigma > \frac{\mathcal{L}_1 + \mathcal{L}_2}{\underline{J}}. \quad (26)$$

renders the set:

$$\mathcal{P} := \{\boldsymbol{\rho} \in \mathbb{R}^n : \|\boldsymbol{\rho}\| \leq \widetilde{\rho}\},$$

an Robust Control Invariant [12] set for the error dynamics (23), with:

$$\widetilde{\rho} := \frac{\tilde{\xi}}{\sigma \underline{J} - \mathcal{L}_1 - \mathcal{L}_2} > 0.$$

**Proof :** Consider the positive definite function $\Lambda(\boldsymbol{\rho}) = \frac{1}{2}\|\boldsymbol{\rho}\|^2$. The time derivative of $\Lambda$ along the trajectories of the system (23) is given by:

$$\begin{aligned} \dot{\Lambda}(\boldsymbol{\rho}) &= \boldsymbol{\rho}^\top \dot{\boldsymbol{\rho}} \\ &= \boldsymbol{\rho}^\top [h(\boldsymbol{e}, \hat{\boldsymbol{v}}) - h(\hat{\boldsymbol{e}}, \hat{\boldsymbol{v}})] + \boldsymbol{\rho}^\top [\zeta(\boldsymbol{e}, \dot{\boldsymbol{p}}_d) - \zeta(\hat{\boldsymbol{e}}, \dot{\boldsymbol{p}}_d)] \\ &\quad + \boldsymbol{\rho}^\top J(\boldsymbol{e}, \boldsymbol{p}_d)(\boldsymbol{v} - \hat{\boldsymbol{v}}) + \boldsymbol{\rho}^\top \xi(\boldsymbol{e}, \boldsymbol{\omega}). \end{aligned}$$

By employing (24a)-(24b) and the boundedness of $\|\xi(\cdot)\|$ given in Remark 2, i.e, $\|\xi(\boldsymbol{e},\boldsymbol{\omega})\| \leq \widetilde{\xi}$, $\widetilde{\xi} > 0$, the latter becomes:

$$\dot{\Lambda}(\boldsymbol{\rho}) \leq (\mathcal{L}_1 + \mathcal{L}_2)\|\boldsymbol{\rho}\|^2 + \boldsymbol{\rho}^\top J(\boldsymbol{e},\boldsymbol{p}_d)(\boldsymbol{v}-\hat{\boldsymbol{v}}) + \widetilde{\xi}\|\boldsymbol{\rho}\|. \quad (27)$$

Now, by taking $J = \frac{J+J^\top}{2} + \frac{J-J^\top}{2}$; using the fact that $y^\top \frac{J-J^\top}{2} y = 0$, $\forall y$; and substituting the control law (25), the inequality of (27) yields:

$$\dot{\Lambda}(\boldsymbol{\rho}) \leq \left[-(\sigma \underline{J} - \mathcal{L}_1 - \mathcal{L}_2)\|\boldsymbol{\rho}\| + \widetilde{\xi}\right] \|\boldsymbol{\rho}\|.$$

Thus, it holds that:

$$\dot{\Lambda}(\boldsymbol{\rho}) < 0 \text{ when } \|\boldsymbol{\rho}\| > \frac{\widetilde{\xi}}{\sigma \underline{J} - \mathcal{L}_1 - \mathcal{L}_2}. \quad (28)$$

Moreover, owing to the fact that $\boldsymbol{\rho}(0) = 0$, we have:

$$\|\boldsymbol{\rho}(t)\| \leq \frac{\widetilde{\xi}}{\sigma \underline{J} - \mathcal{L}_1 - \mathcal{L}_2}, \ \forall t \geq 0.$$

which concludes the proof. □

A graphical illustration of the proposed tube based control strategy is given in Fig 2. Under the proposed control scheme (21), the real trajectory $\boldsymbol{e}(t)$ lies inside the hyper-tube which is centered along the nominal trajectory $\hat{\boldsymbol{e}}$ with radius $\widetilde{\rho}$ for all times, i.e., $\|\boldsymbol{\rho}(t)\| \leq \widetilde{\rho}$, $\forall t \in \mathbb{R}_{\geq 0}$.

### C. Online Optimal Control

As mentioned before, the control action $\hat{\boldsymbol{v}}(\hat{\boldsymbol{e}})$ in eq. (21) will be the outcome of a FHOCP solved for the nominal dynamics eq. (20). In this respect, consider a sequence of sampling times $\{t_k\}$, $k \in \mathbb{N}$, with a constant sampling period $0 < \delta_t < T$, where $T$ is a prediction horizon such that $t_{k+1} := t_k + \delta_t$, $\forall k \in \mathbb{N}$. At each sampling time $t_k$, a FHOCP is solved as follows:

$$\min_{\hat{\boldsymbol{v}}(\cdot)} \left\{ \|\hat{\boldsymbol{e}}(t_k+T)\|_P^2 + \int_{t_k}^{t_k+T} \left[ \|\hat{\boldsymbol{e}}(\mathfrak{s})\|_Q^2 + \|\hat{u}(\mathfrak{s})\|_R^2 \right] d\mathfrak{s} \right\} \quad (29a)$$

subject to:

$$\dot{\hat{\boldsymbol{e}}}(\mathfrak{s}) = J(\hat{\boldsymbol{e}}(\mathfrak{s}),\boldsymbol{p}_d)\hat{\boldsymbol{v}} + \zeta(\hat{\boldsymbol{e}}(\mathfrak{s}),\dot{\boldsymbol{p}}_d), \quad \hat{\boldsymbol{e}}(t_k) = \boldsymbol{e}(t_k), \quad (29b)$$

$$\hat{\boldsymbol{e}}(\mathfrak{s}) \in \overline{\mathcal{E}}, \quad \hat{\boldsymbol{v}}(\mathfrak{s}) \in \overline{V}, \quad \forall \delta_{\mathfrak{t}} \in [t_k, t_k+T], \quad (29c)$$

$$\hat{\boldsymbol{e}}(t_k+T) \in \mathcal{F}, \quad (29d)$$

where $Q$, $P \in \mathbb{R}^{3\times 3}$ and $R \in \mathbb{R}^{3\times 3}$ are positive definite gain matrices. Moreover, $\overline{\mathcal{E}}$, $\overline{V}$ and $\mathcal{F}$ are designing sets that are defined in order to guarantee that while the solution of FHOCP (29a)-(29d) is derived for the nominal dynamics (20), the real trajectory $\boldsymbol{e}(t)$ and control inputs $\boldsymbol{v}(t)$ satisfy the corresponding state and input constraint sets $\mathcal{E}$ and $V$ respectively. More specifically, the following modification is performed:

$$\overline{\mathcal{E}} := \mathcal{E} \ominus \mathcal{P}, \quad \overline{V} := V \ominus [-\sigma \circ \mathcal{P}]. \quad (30)$$

This intuitively means that the sets $\mathcal{E}$, $V$ are tightened accordingly, in order to guarantee that while the nominal states $\hat{\boldsymbol{e}}$ and the nominal control input $\hat{\boldsymbol{v}}$ are calculated, the corresponding real error states $\boldsymbol{e}$ and real control input $\boldsymbol{v}$ satisfy the state and input constraints $\mathcal{E}$, $\mathcal{P}$ and $\mathcal{U}$, respectively. Define the *terminal set* by:

$$\mathcal{F} := \left\{ \hat{\boldsymbol{e}} \in \overline{\mathcal{E}} : \|\hat{\boldsymbol{e}}\|_P \leq \bar{\epsilon} \right\}, \quad \bar{\epsilon} > 0, \quad (31)$$

which is employed here in order to enforce the stability of the system [10].

*Newly Detected Obstacles:* as mentioned before, the obstacles within the workspace may be detected online by the vehicle's on–board sensors (e.g., multi–beam imaging or side scan sonar). In such a case, it should be assured that the solution of the FHOCP corresponds to the region that is accessible by the sensing capabilities of the vehicle. This intuitively means it is required any potential new obstacles to be visible by the vehicle even in the worst case (i.e., maximum velocity of the robot under maximum disturbances). Thus, assuming that $\bar{R}$ denotes the sensing range of the system as it is already stated in Section-III-B, the prediction horizon $T$ should be set as follows:

$$T \leq \frac{\bar{R}}{\bar{V} + \widetilde{\xi}} \quad (32)$$

where $\bar{V}$ is defined in (11).

**Remark 3:** The detection range of these sonar sensors (i.e., $\tilde{R}$) depends on many factors, including the frequency. Low frequency sonars can detect objects at very long distance, depending on the sound propagation environment. Medium frequency sonars (typically operating between $7.5kHz$ and up to $30kHz$) can detect a object at a multiple nautical miles. On the other hands, high frequency sonars ($> 100kHz$), typically used for underwater inspection can detect smaller objects at a few hundreds meters (i.e., $> 100m$). Thus, in view of (11), in a real scenario the predefined upper bound of the vehicle velocity can be tuned accordingly to the capability sensing range $\tilde{R}$ of the available sonar system in order to get an valuable prediction horizon enough for solving the FHOCP (29a)-(29d).

Now we are ready to state the main result of this work:

**Theorem 1:** Suppose that at time $t = 0$ the FHOCP (29a)-(29d) is feasible. Then, the proposed feedback control law (21), (25), renders the closed-loop system Input-to-State stable (ISS) with respect to the disturbances, for every initial condition $\hat{\boldsymbol{e}}(0) \in \mathcal{E}$.

*Proof:* The proof of the theorem follows similar arguments presented in our previous work [13]. Due to the fact that only the state of the nominal system is used while the FHOCP (29a)-(29d) is solved, the on-line optimization does not depend on the disturbances. Thus, the *feasibility proof* follows same arguments as in [10], [13] and is omitted here. Regarding the *convergence analysis*, due to the fact that the set $\mathcal{P}$ is an RPI set, it holds that:

$$\|\boldsymbol{\rho}(t)\| \leq \widetilde{\rho}, \forall t \geq 0. \quad (33)$$

Due to the asymptotic stability of the nominal system, there exists a class $\mathcal{KL}$ function $\beta$ such that:

$$\|\hat{\boldsymbol{e}}(t)\| \leq \beta(\|\hat{\boldsymbol{e}}(0)\|, t), \forall t \geq 0. \quad (34)$$

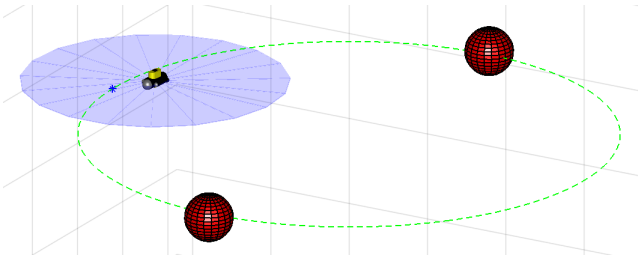

**Fig. 3:** Simulation setup: The sensing range of the robot is indicated by a blue circle region around the robot. The desired trajectory is depicted with green dashed line which coincides with obstacles positions.

By combining (22), (33) and (34), we get:

$$\|\boldsymbol{e}(t)\| \leq \beta(\|\hat{\boldsymbol{e}}(0)\|, t) + \widetilde{\rho},$$

for every $t \geq 0$, which leads to the conclusion of the proof. ■

## V. Simulation Results

The simulation results were conducted using a dynamic simulation environment built in MATLAB with sampling time $0.1sec$. We considered a scenario with two obstacles which lie in $\boldsymbol{p}_1 = [3,\ 0,\ 0]^\top$ and $\boldsymbol{p}_2 = [-3,\ 0,\ 0]^\top$ respectively. The desired trajectory is a circle in horizontal plane defined by $\boldsymbol{p}_d(t) = [3\sin(\frac{\pi}{25}t), 3\cos(\frac{\pi}{25}t), 0]^T$. Notice that the desired trajectory coincides with obstacles positions. The predefined upper bound of the vehicle velocities are defined as: $\bar{u} = 0.4\frac{m}{s}$, $\bar{w} = 0.3\frac{m}{s}$ and $\bar{r} = 0.5\frac{rad}{s}$. Moreover, the capability sensing range and the horizon of the FHOCP are considered as $\bar{R} = 1.5$ and $T = 8 * dt = 0.8\,\text{sec}$ respectively, satisfying the condition (32). Notice that the obstacles are detected and are considered by the controller when they are within the sensing range of the robot. The initial configuration is depicted in Fig 3. In addition, the dynamics of the considered AUV were affected by external disturbances acting along $x$, $y$ and $z$ axes modeled by the corresponding velocities $\omega_1 = 0.1\sin(2\frac{\pi}{15}t)\frac{m}{s}$, $\omega_2 = 0.1\cos(2\frac{\pi}{15}t)\frac{m}{s}$ and $\omega_3 = 0.1\sin(2\frac{\pi}{15}t)\frac{m}{s}$. Furthermore, the parameter $\epsilon$ defined in (15) is set to $\epsilon = 0.1$. The simulation scenario has been conducted over a time period of $100\,\text{sec}$ in which the robot is required to avoid the obstacles twice each. The errors and control inputs evolution are depicted in Fig. 4 and Fig. 5 respectively. It can be witnessed that the control input constraints always satisfied and the error $e_d$ remains always greater than $\epsilon = 0.1$, i.e., $e_d(t) \geq \epsilon, \forall t \geq 0$.

## VI. Conclusions and Future Work

This work presents a robust trajectory tracking controller for underactuated AUVs operating in an uncertain and dynamic workspace including obstacles. The workspace knowledge (i.e., obstacles positions) is constantly updated online via the vehicle's sensors. Obstacle avoidance with any of the detected obstacles is guaranteed, despite the presence of external disturbances. Moreover, various constraints such as predefined upper bound of the vehicle velocity are considered during the control design. The closed-loop system has analytically guaranteed stability and convergence properties.

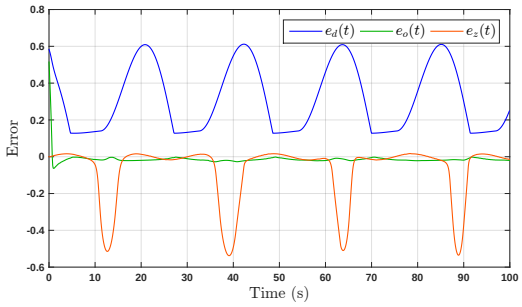


**Fig. 4:** The evolution of the error over time. The peaks in $e_d$ and $e_z$ stand for the fact that the robot is leaving the desired trajectory in order to avoid the obstacles.

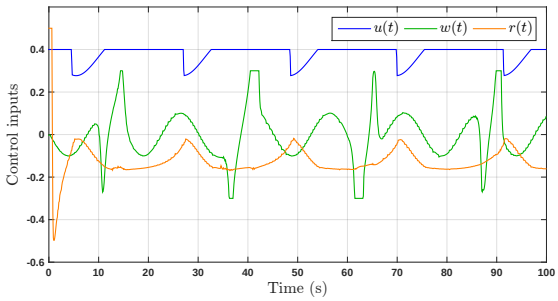


**Fig. 5:** The evolution of the control input signals over time.

Future research efforts will be devoted towards extending the proposed methodology for multiple Autonomous Underwater Vehicles.

## References


[1] S. Heshmati-Alamdari, *Cooperative and Interaction Control for Underwater Robotic Vehicles*. PhD thesis, National Technical University of Athens, 2018.

[2] B. Subudhi, K. Mukherjee, and S. Ghosh, "A static output feedback control design for path following of autonomous underwater vehicle in vertical plane," *Ocean Engineering*, vol. 63, pp. 72–76, 2013.

[3] J. Refsnes, A. Sørensen, and K. Pettersen, "Model-based output feedback control of slender-body underactuated auvs: Theory and experiments," *IEEE Transactions on Control Systems Technology*, vol. 16, no. 5, pp. 930–946, 2008.

[4] C. Petres, Y. Pailhas, P. Patron, Y. Petillot, J. Evans, and D. Lane, "Path planning for autonomous underwater vehicles," *IEEE Transactions on Robotics*, vol. 23, no. 2, pp. 331–341, 2007.

[5] S. Heshmati-Alamdari, A. Nikou, and D. V. Dimarogonas, "Robust trajectory tracking control for underactuated autonomous underwater vehicles," *https://arxiv.org/abs/1908.10175*, 2019.

[6] *The Society of Naval Architects and Marine Engineers, Nomenclature for treating the motion of a submerged body through a fluid (Technical and Research Bulletin No 105)*, 1950.

[7] T. Fossen, "Guidance and control of ocean vehicles," *Wiley, New York*, 1994.

[8] D.Panagou and K. J. Kyriakopoulos, "Control of underactuated systems with viability constraints," *Proc. of the 50th IEEE Conference on Decision and Control and European Control Conference*, pp. 5497–5502, 2011.

[9] D. Koditschek and E. Rimon, "Robot navigation functions on manifolds with boundary," *Advances in Applied Mathematics*, vol. 11, no. 4, pp. 412–442, 1990.

[10] H. Chen and F. Allgöwer, "A Quasi-Infinite Horizon Nonlinear Model Predictive Control Scheme with Guaranteed Stability," *Automatica*, vol. 34, no. 10, pp. 1205–1217, 1998.

[11] D. Mayne, J. Rawlings, C. Rao, and P. Scokaert, "Constrained Model Predictive Control: Stability and Optimality," *Automatica*, vol. 36, no. 6, pp. 789–814, 2000.

[12] H. K. Khalil, "Nonlinear Systems," *Prentice Hall*, 2002.

[13] A. Nikou and D. V. Dimarogonas, "Decentralized Tube-based Model Predictive Control of Uncertain Nonlinear Multi-Agent Systems," *International Journal of Robust and Nonlinear Control (IJRNC), https://arxiv.org/abs/1808.05408*, 2019.